Evolution of Fermi surface by electron filling into a free-electronlike surface state

Iwao Matsuda,* Toru Hirahara, Mitsuru Konishi, Canhua Liu, Harumo Morikawa, Marie D'angelo, and Shuji Hasegawa
Department of Physics, School of Science, The University of Tokyo, 7-3-1 Hongo, Bunkyo-ku, Tokyo 113-0033, Japan

Taichi Okuda and Toyohiko Kinoshita
Synchrotron Radiation Laboratory, Institute for Solid State Physics, The University of Tokyo, 5-1-5 Kashiwanoha, Kashiwa 277-8581, Japan

(Received 10 September 2004; revised manuscript received 18 January 2005; published 16 June 2005)

We have studied the evolutions of surface electronic structure (Fermi surfaces and valence bands) by electron filling into a two-dimensional free-electronlike surface state, during adsorptions of monovalent metal atoms (noble metal; Ag, and alkali metal; Na) on the Si(111)$\sqrt{3}\times\sqrt{3}$-Ag surface. The Fermi surfaces (Fermi rings) of a small electron pocket grow continuously with the adsorption. Eventually, when the $\sqrt{21}\times\sqrt{21}$ superstructure was formed by 0.1–0.2 monolayer adsorption of Ag or Na, the Fermi ring is found to be larger than the $\sqrt{21}\times\sqrt{21}$-surface Brillouin zone (SBZ), and to be folded by obeying the $\sqrt{21}\times\sqrt{21}$ periodicity. As a result, the Fermi surface is composed of a large hole pocket at the $\bar{\Gamma}$ point and small electron pockets at the $\bar{K}$ point in each reduced $\sqrt{21}\times\sqrt{21}$ SBZ, meaning that the behavior of surface-state carriers becomes hole-like. Despite a sharp chemical distinction between the adsorbates, a very similar surface electronic structure is found for both the Ag-induced and Na-induced $\sqrt{21}\times\sqrt{21}$ phases. Based on the Boltzmann equation, surface-state conductivites of these surfaces are obtained from the measured Fermi surfaces, reproducing successfully the results of previous surface transport measurements.

DOI: 10.1103/PhysRevB.71.235315 PACS number(s): 79.60.−i, 68.35.−p, 73.20.−r

I. INTRODUCTION

Surface superstructures formed by adsorptions of alkali metals or noble metals on semiconductor crystals have been intensively studied as prototype systems of metal/semiconductor interfaces for a long time, because of simple electronic structures of the adsorbates.[1–4] But they have turned out to be very complicated in the electronic and atomic structures and contain rich physics. The Si(111)$\sqrt{3}\times\sqrt{3}$-Ag surface superstructure, which is formed by one monolayer (ML) Ag adsorption on a Si(111) surface, is one of the most popular, for which almost all kinds of surface-science techniques have been applied and its atomic and electronic structures are now well understood.[5–8] It has an isotropic two-dimensional free-electronlike surface state. Adsorption of monovalent atoms on this surface, furthermore, has attracted considerable interests because adsorption of tiny amounts of monovalent atoms on this surface is reported to produce electron filling into the surface state, resulting in a high surface electrical conductivity.[1,9]

When the coverage of the monovalent adatoms reaches certain values (0.1–0.2 ML) on the $\sqrt{3}\times\sqrt{3}$-Ag surface, $\sqrt{21}\times\sqrt{21}(\pm R10.89°)$ phases are known to appear, which are regarded as a model of binary surface alloys on semiconductors.[1,10–14] Since the $\sqrt{21}\times\sqrt{21}$ phases induced by noble-metal adsorptions show high electrical conductivities, they are nowadays an important playground to investigate surface-state electrical conduction, i.e., electronic transport through the topmost atomic layer on a crystal.[1,15,16] Since the conductivity is directly related to the surface electronic structure, several researches of angle- resolved photoemission spectroscopy (ARPES) have been performed.[1,10–13] The Si(111)$\sqrt{21}\times\sqrt{21}$-(Ag,Au) and Si(111)$\sqrt{21}\times\sqrt{21}$-Ag surface superstructures, which are induced by depositing about 0.2 ML Au or Ag on the Si(111)$\sqrt{3}\times\sqrt{3}$-Ag surface, respectively, are found to possess surface-state bands dispersing across the Fermi level (E_F). Such metallic bands are believed to bring about the high surface conductivity. Based on scanning tunneling microscopy (STM) images, several structure models with different adatom coverages are proposed so far for these noble-metal induced $\sqrt{21}\times\sqrt{21}$ surfaces. A recent x-ray diffraction study have shown that, among them, the structure models with adatom coverage of 0.24 ML (five adatoms in the $\sqrt{21}\times\sqrt{21}$ unit cell) are favored.[14]

In contrast to the varieties of researches on the noble-metal adsorption, there exists a limited number of reports for the alkali-metal induced $\sqrt{21}\times\sqrt{21}$ superstructures; only a high surface conductivity and STM images are reported.[1,17] Thus, the further researches on the alkali-metal induced ones, especially on the electronic structure, are highly requested for binary chemistry as well as for the future surface transport studies with sophisticated microfour-point probes and four-tip STM probes.[18–20]

In the present research, we have performed comprehensive studies on both of the noble-and alkali-metal adsorptions on the Si(111)$\sqrt{3}\times\sqrt{3}$-Ag in order to acquire a general picture on electronic properties of the monovalent-atom-induced $\sqrt{21}\times\sqrt{21}$ phases. We have chosen Ag and Na atoms because they have the simplest electronic states among noble and alkali metals, respectively, and they do not diffuse into bulk Si substrate.[4,21] To make detailed comparisons, important parameters of alkali- and noble-metal atoms are summarized in Table I.[22] As is well known, sharp distinctions are identified between the two groups of monovalent atoms con-

TABLE I. Parameters of various monovalent atoms (Ref. 22). χ is electronegativity, I_{first} is the first ionization energy (eV), r_{metal} is atomic radius (Å), and r_{ion} is ionic radius (Å).

	χ	I_{first}	r_{metal}	r_{ion}
		Alkali Metal		
Cs	0.79	3.894	2.67	1.67–1.88
Rb	0.82	4.177	2.48	1.52–1.72
K	0.82	4.341	2.35	1.37–1.64
Na	0.93	5.139	1.9	0.99–1.39
		Noble Metal		
Au	2.4	9.226	1.46	1.37
Ag	1.93	7.576	1.44	1.0–1.28
Cu	1.90	7.726	1.28	0.46–0.77

cerning electronegativity and the first ionization energy. On the other hand, a similarity may be found for atomic sizes between Na and Ag (Au) atoms. The ionic radius of Na is almost the same as that of Ag (Au), and the atomic radius is much closer to that of Ag (Au) than those of other alkali metals. Therefore, a comparison between the Ag and Na depositions is effective for studying chemical and physical trends in the adsorption on the $\sqrt{3}\times\sqrt{3}$-Ag surface.

Through detailed electron diffraction observations, we have discovered a $\sqrt{21}\times\sqrt{21}$-(Ag,Na) superstructure around 0.1–0.2 ML Na adsorption at 65–130 K. We have, then, performed ARPES measurements on the $\sqrt{21}\times\sqrt{21}$-(Ag,Na) as well as the $\sqrt{21}\times\sqrt{21}$-Ag surface. Both surfaces are found to be metallic and have very similar band structures. The Fermi surfaces (rings), the surface band dispersions, the substrate band bending, and the surface conductivity are determined. The present research reports a quantitative agreement between results of photoemission spectroscopy and surface transport measurements. The surface structure is discussed by comparing results of the Ag and Na adsorptions.

II. EXPERIMENTS

The ARPES experiments were done with unpolarized He Iα radiation ($h\nu$=21.2 eV) at the laboratory and with linearly polarized synchrotron radiation (SR) at Beamline BL-18A (Institute for Solid State Physics, University of Tokyo, Kashiwa, Japan) of KEK-Photon Factory, Japan.[7] The measurements were performed at 100–130 K with commercial angle-resolved photoelectron spectrometers of Scienta SES-100 (laboratory) and VG ADES 500 (Beamline). A slight energy shift due to the surface photovoltage effect has been calibrated by photoemission signals from bulk Si bands, bulk Si 2*p* core levels, and Fermi edge of the metallic surface superstructures. For experiments with the He Iα radiation, an angle between the directions of incident photons and detecting photoelectrons was fixed to be 50°. The Fermi energy was determined by fitting the Fermi edge measured on a Ta holder attached to the sample.

STM images presented in this paper were obtained at 65 K with a commercial ultrahigh-vacuum low-temperature STM (Unisoku USM-501). The base pressure during all the experiments was better than 1×10^{-10} mbar. Temperature was monitored by thermocouples attached close to the sample on the sample holder.

First, a clean Si(111)7×7 surface was prepared on an *n*-type (2–15 Ω cm) or a *p*-type (1–10 Ω cm) Si(111) wafer by a cycle of *in situ* resistive heat treatments. The Si(111)$\sqrt{3}\times\sqrt{3}$-Ag surface superstructure was made by monolayer Ag deposition at substrate temperature of ~520 °C. This preparation procedure ensured that the $\sqrt{3}\times\sqrt{3}$-Ag superstructure was formed up to the step edges and entirely covered the surface, as confirmed by STM observation.[23] Although a postannealing at a temperature higher than 600 °C was proposed to remove the "residual Ag adatom gas" remaining on the $\sqrt{3}\times\sqrt{3}$-Ag surface,[24] we did not employ the high-temperature annealing, because such a high temperature annealing was found to destroy the $\sqrt{3}\times\sqrt{3}$-Ag structure close to step edges.[23]

The deposition of Ag was done using a graphite effusion cell or an alumina basket. A monolayer, 1 ML, corresponds to 7.83×10^{14} atoms/cm^2, the number density of Si atoms in the topmost layer of the (111) face. The coverage and evaporation rate of Ag were determined by the completion of the Si(111)$\sqrt{3}\times\sqrt{3}$-Ag structure during *in situ* observations of electron diffraction. The quality and cleanliness of the $\sqrt{3}\times\sqrt{3}$-Ag surface was ascertained by sharp $\sqrt{3}\times\sqrt{3}$-electron diffraction (low-energy electron diffraction or reflection high-energy electron diffraction) patterns, and strong surface-state signals in the valence-band photoemission spectra.[7,11–13,25,26] Sodium atoms were evaporated by using commercial SAES-getter sources which were thoroughly outgassed to minimize any impurity effect. The sodium coverage was calibrated through comparisons of the normalized Na 2*s* photoemission intensity, the intensity ratio between two core-level emission lines Na 2*s*/Si 2*p*, work function, and diffraction pattern with those of the δ-7×7 phase prepared by ~1 ML Na deposition on the clean 7×7 surface at room temperature.[21,27–29]

III. RESULTS AND DISCUSSION

It has been reported that ~0.2 ML Ag deposition on the Si(111)$\sqrt{3}\times\sqrt{3}$-Ag surface at temperatures below 200 K results in the formation of a $\sqrt{21}\times\sqrt{21}$ ordered phase.[1,11,12] Figure 1(a) shows a low-energy electron diffraction pattern of the $\sqrt{21}\times\sqrt{21}(\pm R10.89°)$ taken after ~0.15 ML Ag deposition on the $\sqrt{3}\times\sqrt{3}$-Ag surface at ~130 K. We found that the same $\sqrt{21}\times\sqrt{21}(\pm R10.89°)$ diffraction pattern was also obtained by ~0.15 ML Na deposition on the $\sqrt{3}\times\sqrt{3}$-Ag at ~130 K, Fig. 1(b). Morphological details of the phase formation observed by STM will be described elsewhere.[29] A series of normal emission ARPES spectra from the Si(111)7×7, Si(111)$\sqrt{3}\times\sqrt{3}$-Ag, Si(111)$\sqrt{21}\times\sqrt{21}$-Ag and Si(111)$\sqrt{21}\times\sqrt{21}$-(Ag,Na) phases are given in Fig. 1(c). Through the $\sqrt{3}\times\sqrt{3}$-Ag phase formation from the 7×7, the surface-state signals of the 7×7 denoted by SS_1 (adatom

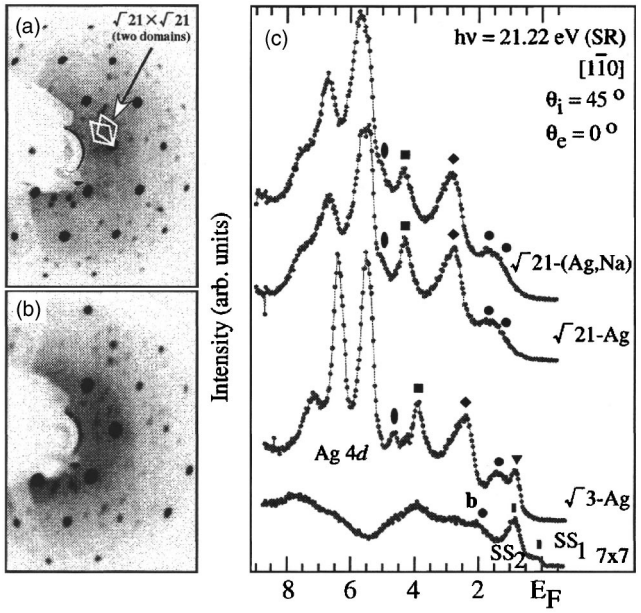

FIG. 1. Low-energy electron diffraction patterns of (a) Si(111)$\sqrt{21}\times\sqrt{21}$-Ag and (b) Si(111)$\sqrt{21}\times\sqrt{21}$-(Ag,Na) taken at electron energy of ~90 eV. Unit cells of $\sqrt{21}\times\sqrt{21}(\pm R10.89°)$ are indicated by white lines. (c) A set of normal emission ARPES spectra for Si(111)7×7 (7×7), Si(111)$\sqrt{3}\times\sqrt{3}$-Ag ($\sqrt{3}$-Ag), Si(111)$\sqrt{21}\times\sqrt{21}$-Ag ($\sqrt{21}$-Ag), and Si(111)$\sqrt{21}\times\sqrt{21}$-(Ag,Na) ($\sqrt{21}$-(Ag,Na) . The spectra were taken with synchrotron radiation (SR) of $h\nu=21.2$ eV along [$1\bar{1}0$] azimuth. The incident angle of photon (θ_i) was 45°.

state) and SS_2 (rest-atom state) perish and various electronic states, especially sharp Ag 4*d* peaks at binding energy (E_B) of ~6 eV, appear.[7,11–13,25,26] Comparison of spectra between the $\sqrt{3}\times\sqrt{3}$ and $\sqrt{21}\times\sqrt{21}$ phases indicates a drastic change of electronic structure near E_F. On the other hand, the states of the $\sqrt{3}\times\sqrt{3}$ phase at $E_B=2-5$ eV persist in the $\sqrt{21}\times\sqrt{21}$ band diagram, but shift slightly toward higher binding energies. Through the transition from the $\sqrt{3}\times\sqrt{3}$ to $\sqrt{21}\times\sqrt{21}$ phases, ARPES peaks of the Ag 4*d* levels have become broader. In this paper, the electronic structure of the Si(111)$\sqrt{21}\times\sqrt{21}$-Ag and Si(111)$\sqrt{21}\times\sqrt{21}$-(Ag,Na) are described in three different energy regions, Fermi level region (Fermi surface), valence band region (down to $E_B\sim5$ eV), and Ag 4*d* band region ($E_B=5\sim8$ eV), separately. Finally, the surface-state electrical conductivity is discussed by combining the Fermi surface and band bending results.

A. Fermi rings

Figure 2 shows the evolution of Fermi surface (Fermi rings) by Ag (Na) adsorptions on the Si(111)$\sqrt{3}\times\sqrt{3}$-Ag surface at ~120 K. The measurements were performed with He Iα radiation and the data acquisition was made by recording the photoelectron intensity at E_F while scanning emission angles to produce the Fermi surface maps. In the figure, the large photoemission intensity is colored black. The energy contour at E_F of the pristine $\sqrt{3}\times\sqrt{3}$-Ag phase, Fig. 2(a), is shown as a circle centered at the $\bar{\Gamma}_{\sqrt{3}}$ point with a radius $k_F\sim0.1$ Å^{-1}, indicating isotropic metallic nature of the surface state. Despite the $\sqrt{3}\times\sqrt{3}$ periodicity, the Fermi ring is observed in the second, but not in the first surface Brillouin zones (SBZ).[10] This phenomenon was successfully reproduced by a calculation of the optical transition matrix based on a simple tight-binding approximation for the surface topmost-layer Ag atoms; the intensity of the surface-state emission in the first SBZ is diminished by destructive interferences in the matrix elements (i.e., photoemission structure factor effect). The details of the isotropic band dispersion and the effect is described elsewhere.[30,31] Especially, the band composing the Fermi surface is known to have a parabolic energy dispersion with an effective mass of $m^*=0.13m_e$, meaning a two-dimensional free electronlike state.[30]

After 0.07 ML Ag deposition on the $\sqrt{3}\times\sqrt{3}$-Ag surface, the Fermi ring is enlarged to $k_F\sim0.2$ Å^{-1} as shown in Fig. 2(b), implying electron transfer from the Ag adsorbates to the surface state.[9] Further deposition up to 0.15 ML results in a formation of the $\sqrt{21}\times\sqrt{21}$ phase and the corresponding Fermi rings are shown in Fig. 2(c). We can find a dark circle (the radius being ~0.26 Å) which is larger than that in Fig. 2(b), and additionally we can observe parts of the Fermi circles superimposed with each other in the whole observed *k* space.

In Fig. 3(a), the Fermi ring of the $\sqrt{21}\times\sqrt{21}$ surface is drawn on an extended $\sqrt{21}\times\sqrt{21}$-surface Brillouin zone (SBZ). Since the Fermi ring is larger than the first SBZ, the first SBZ is fully filled with electrons. The Fermi ring covers up to the third SBZs and the segments of the Fermi ring in the second and third SBZs are depicted in Figs. 3(b) and 3(c), respectively. The Fermi ring of the second SBZ consists of a hole pocket centered at the $\bar{\Gamma}_{\sqrt{21}\times\sqrt{21}}$ point, while that of the third SBZ is composed of electron pockets at the $\bar{K}_{\sqrt{21}\times\sqrt{21}}$ points. On the Si(111)$\sqrt{21}\times\sqrt{21}$-Ag surface, there are two domains of the $\sqrt{21}\times\sqrt{21}$ periodicity which are rotated by 21.78° to each other (Fig. 1). Therefore, the photoemission result in Fig. 2(c) is an overlap of the Fermi rings coming from these two domains as shown in Figs. 3(d) and 3(e). By taking these facts into account, these Fermi rings are tiled on the experimentally mapped ones as shown in Fig. 2(d). As obviously shown in the figure, the experimental result is well reproduced by the Fermi rings superimposed by obeying the $\sqrt{21}\times\sqrt{21}$ periodicity. This means that this surface state comes from the $\sqrt{21}\times\sqrt{21}$ superstructure. The photoemission intensity of the rings is modulated due to the photoemission matrix element effects.

Since, as mentioned above, the Fermi rings in Fig. 2(c) are a result of the band folding of a large Fermi ring in the $\sqrt{21}\times\sqrt{21}$ SBZs, the Fermi ring is not a simple isotropic free-electronlike state anymore, rather composed of electron and hole pockets. The spectral weight of photoelectrons is peaked at envelopes of the electron and hole pockets, resulting in the circle.[32] Therefore, the radius of the large circle corresponds to the Fermi wave vector of the original free-electron band. The electron density n_{2D} can be related to k_F by

$$k_F=\sqrt{2\pi n_{2D}}. \quad (1)$$

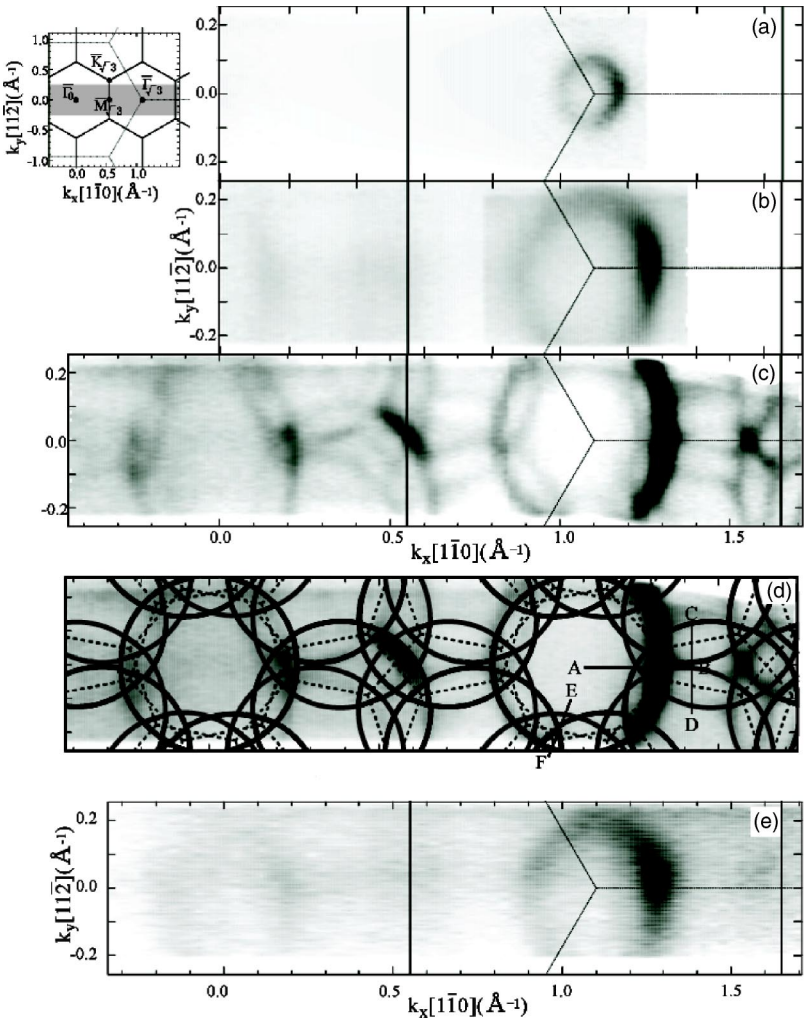

FIG. 2. Evolutions of the Fermi rings by Ag or Na deposition on Si(111)$\sqrt{3}\times\sqrt{3}$-Ag at ~120 K. The additional Ag coverage is (a) 0 ML [the pristine Si(111)$\sqrt{3}\times\sqrt{3}$-Ag], (b) 0.07 ML, and (c) 0.15 ML [the Si(111)$\sqrt{21}\times\sqrt{21}$-Ag.] The data were taken with He Iα radiation. A schematic drawing of the surface Brillouin zone (SBZ) of $\sqrt{3}\times\sqrt{3}$ with symmetry points are shown in the inset. The SBZs of 1×1 and $\sqrt{3}\times\sqrt{3}$ are drawn as thick and thin lines, respectively. The measured region of (c) is depicted as shaded area. (d) Tiling of the Fermi rings and SBZs of the two $\sqrt{21}\times\sqrt{21}$ domains, overlapped on the experimental result of (c). Three straight lines (A-B, C-D, and E-F) in (d) are scanning axes of ARPES measurements shown in Fig. 5. A photoemission Fermi surface map of the Si(111)$\sqrt{21}\times\sqrt{21}$-(Ag,Na) surface prepared by Na deposition at ~120 K is shown in (e).

Then, the n_{2D} can be calculated from the k_F values, 0.16, 0.64, and 1.1×10^{14} cm^{-2} for the pristine $\sqrt{3}\times\sqrt{3}$ [Fig. 2(a)], the 0.07-ML-added surface [Fig. 2(b)], and the $\sqrt{21}\times\sqrt{21}$-Ag [Fig. 2(c)], respectively. One can find that the increase in electron density is nearly proportional to the additional Ag coverage. The electron density of the $\sqrt{21}\times\sqrt{21}$ phase approximately corresponds to three electrons in the $\sqrt{21}\times\sqrt{21}$-unit cell. It is worth noting a similarity between the present result and the Fermi surfaces of bulk aluminium or indium which contains three electrons in a unit cell.[33]

Let us, now, move on to the Fermi rings of the Na-induced Si(111)$\sqrt{21}\times\sqrt{21}$-(Ag,Na) surface. The experimental result is shown in Fig. 2(e). A large circle is identified in the second $\sqrt{3}\times\sqrt{3}$ SBZ, while a faint circle is also seen in the first SBZ. Compared to the Fermi surface map of the Si(111)$\sqrt{21}\times\sqrt{21}$-Ag [Fig. 2(c)], the Fermi ring for the Si(111)$\sqrt{21}\times\sqrt{21}$-(Ag,Na) has a smaller k radius with a broader k width. To find the reason for the difference between the two $\sqrt{21}\times\sqrt{21}$ phases, we have performed STM observations. Figure 4 shows STM images of the $\sqrt{21}\times\sqrt{21}$-(Ag,Na) surface taken at 65 K. Through the various Na coverage (0–1 ML), we have found formations of only small patches of the $\sqrt{21}\times\sqrt{21}$-(Ag,Na) domains at the coverage around 0.2 ML.[29] In the STM images taken at the tip bias smaller (larger) than ~1 V, the $\sqrt{21}\times\sqrt{21}$-(Ag,Na) domains are separated by "$\sqrt{3}\times\sqrt{3}$" domains (nanometer-scale protrusions). The protrusions are likely Na clusters formed on the Si(111)$\sqrt{3}\times\sqrt{3}$-Ag surface. Details of the STM observation are reported elsewhere.[29] On the contrary, the Si(111)$\sqrt{21}\times\sqrt{21}$-Ag surface is fully covered by large $\sqrt{21}\times\sqrt{21}$ domains of the $\sqrt{21}\times\sqrt{21}$-Ag phase as reported in the previous research.[12] Therefore, we attribute the differences in the Fermi rings between Figs. 2(c) and 2(e) to their surface morphologies. Namely, while the E_F contour measured by photoemission spectroscopy of Si(111)$\sqrt{21}\times\sqrt{21}$-Ag are originated only from $\sqrt{21}\times\sqrt{21}$ domains, those of $\sqrt{21}\times\sqrt{21}$-(Ag,Na) are from both $\sqrt{21}\times\sqrt{21}$ and Na-cluster-covered "$\sqrt{3}\times\sqrt{3}$" domains. The following discussion is given below.

B. Valence band dispersion

Figure 5 shows three series of ARPES spectra and dispersion curves observed along three lines indicated in k space in Fig. 2(d) for the Si(111)$\sqrt{21}\times\sqrt{21}$-Ag surface. The ARPES spectra taken along the line A-B corresponds to those along $[\bar{1}10]$ direction. As reported previously, in the energy region above $E_B\sim0.8$ eV, there are two surface-state bands, S_4 and S_1.[11] The notation of the surface states are based on this

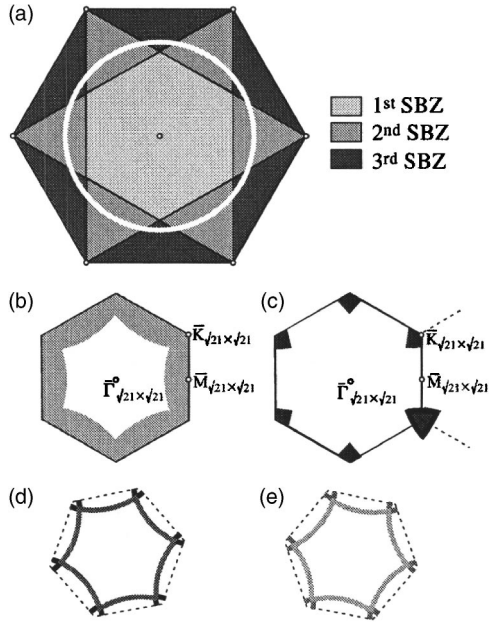

FIG. 3. (a) Superposition of a free-electron ring for valence 3 on an extended hexagonal Brillouin zone. (b) The Fermi rings in the second Brillouin zone. (c) The Fermi rings in the third Brillouin zone. (b) and (c) are given in a reduced zone scheme. The shaded areas correspond to electron-filled regions. (d), (e) The Fermi rings in the two different $\sqrt{21}\times\sqrt{21}$ domains with ±10.89° rotation.

previous report.[11] In the energy-versus-wave-vector diagrams along the lines C-D and E-F, the logarithmic intensities of the spectral features are represented by the darkness in the gray scale. As shown in Fig. 2, a diagram along the C-D direction has photoemission signals only from the hole pocket of the S_4 band. At the zone boundaries (ZBs) of the $\sqrt{21}\times\sqrt{21}$ SBZ ("relative wave vector"=0.087 Å^{-1}), one can obviously find that the S_4 state is energetically separated from the S_1 by 0.1–0.2 eV at $E_B\sim 0.3$ eV. This energy splitting at the zone boundary is consistent with a picture

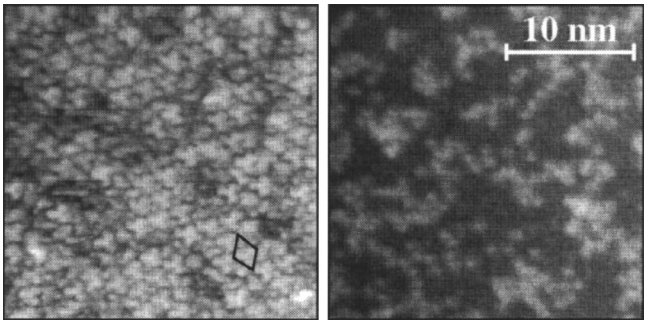

FIG. 4. Filled-state STM images of a surface prepared by ~0.15 ML Na deposition on Si(111)$\sqrt{3}\times\sqrt{3}$-Ag at ~65 K. The left and right images were taken at the same area with tip bias of 0.5 and 3.0 V, respectively. The black lozenge indicates the $\sqrt{21}\times\sqrt{21}$ unit cell.

of band folding and the multiple rings observed in Fig. 2(c) with the $\sqrt{21}\times\sqrt{21}$ periodicity. The Fermi rings shown in Figs. 2(c) and 2(d) are composed of the S_4 band. Along the line E-F which passes through the electron pocket in the third SBZ, the band dispersion shows a similar energy gap (~0.1 eV) at the zone boundary ("relative wave vector" =0.36Å^{-1}). The electron pocket is also composed of the S_4 band.

Figure 6 shows sets of ARPES spectra taken along (a), (b) $[1\bar{1}0]$ and (c) $[11\bar{2}]$ directions from the Si(111)$\sqrt{21}\times\sqrt{21}$-(Ag,Na) surface at hν=21.2 eV. In Fig. 6(a), sharp dispersing bands, for example denoted by **b**, are conspicuously observed at $E_B=2\sim 5$ eV. As shown in Fig. 6(b), in the energy range from E_F to $E_B=0.8$ eV, there are also two bands, S_4' and S_1' [we use primes for names of the surface states of $\sqrt{21}\times\sqrt{21}$-(Ag,Na) phase]. At the zone boundaries in the $\sqrt{21}\times\sqrt{21}$ SBZ (the emission angle $\theta_e=38\sim 39°$ along the $[1\bar{1}0]$ axis), the two bands are energetically separated by ~0.2 eV at $E_B\sim 0.3$ eV. The energy splitting at the zone boundary is also consistent with the discussion for the Ag-induced $\sqrt{21}\times\sqrt{21}$ surface, and

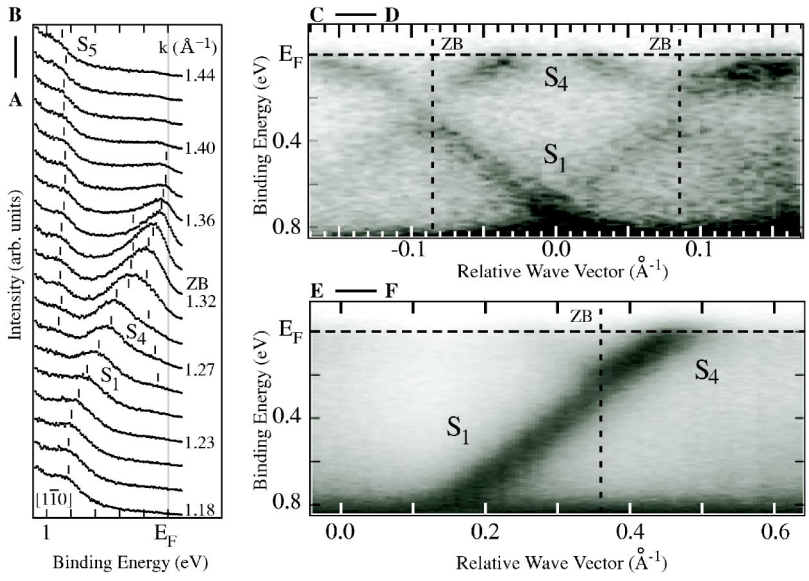

FIG. 5. A series of ARPES spectra and photoemission dispersion plots for the Si(111)$\sqrt{21}\times\sqrt{21}$-Ag surface. The data sets have been compiled from photoemission spectra by mapping angle scans along lines A-B, C-D, and E-F indicated in Fig. 2(d). The dispersion plots are represented with the photoemission intensities in a logarithmic gray scale. The data set has been taken with He Iα radiation. The zone-boundaries (ZB) of the $\sqrt{21}\times\sqrt{21}$ SBZ are indicated.

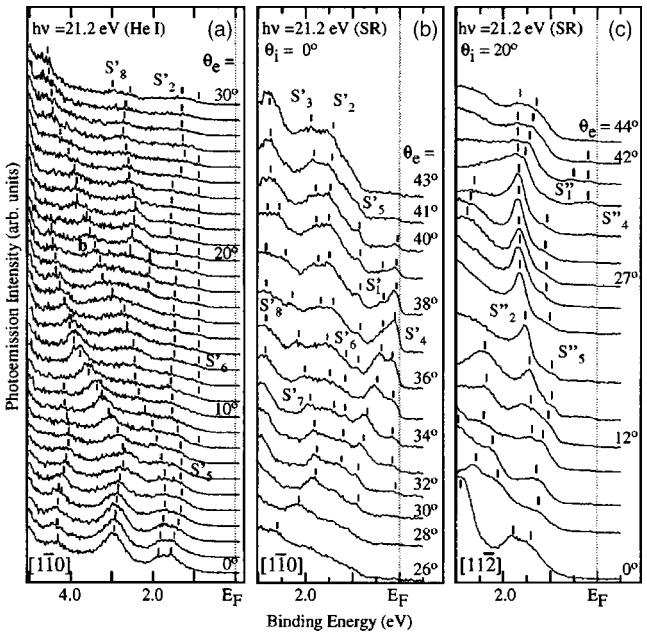

FIG. 6. A collection of ARPES spectra for the Si(111)$\sqrt{21}\times\sqrt{21}$-(Ag,Na) surface taken along (a), (b) $[1\bar{1}0]$ and (c) $[11\bar{2}]$ directions with changes of emission angles (θ_e's). The spectra shown in (a) are taken with He Iα radiation while those in (b) and (c) are taken with synchrotron radiation (SR) at $h\nu$=21.2 eV. A plane of surface normal and incident photon direction is (a), (b) parallel and (c) perpendicular to the one of surface normal and photoelectron detecting direction.

the Fermi rings of the surface are composed of the S_4' band, too. Figure 7 shows the summaries of ARPES spectra presented by band-dispersion curves along the $[1\bar{1}0]$ direction for (a) Si(111)$\sqrt{3}\times\sqrt{3}$-Ag, (b) Si(111)$\sqrt{21}\times\sqrt{21}$-Ag, (c) Si(111)$\sqrt{21}\times\sqrt{21}$-(Ag,Na), and along the $[11\bar{2}]$ direction for (d) Si(111)$\sqrt{21}\times\sqrt{21}$-(Ag,Na). The bulk valence band maximum (VBM) of the Si(111)$\sqrt{3}\times\sqrt{3}$-Ag surface is at $\sim$0.16 eV below E_F, and the bulk band projection region into the 1×1 SBZ is depicted by the shadow in Fig. 7(a).[1,12,34–36] From a comparison between the ARPES results of Si(111)7×7 (not shown), the dispersing bands at E_B=2–5 eV in the shaded region are likely assigned to the Si bulk bands. For example, a band labeled by **b** is associated with a direct transition from the uppermost Si(111) bulk band of Λ_3 symmetry.[37–39] Within the bulk band gap, there are five surface states: $S_1^{\sqrt{3}}$, $S_2^{\sqrt{3}}$, $S_3^{\sqrt{3}}$, $S_4^{\sqrt{3}}$, and $S_5^{\sqrt{3}}$, as reported previously.[7,10–12,25,26,30,31] The Fermi ring in Fig. 2(a) is originated from the $S_1^{\sqrt{3}}$ band.[30,31] Through the Si(111)$\sqrt{21}\times\sqrt{21}$-Ag or Si(111)$\sqrt{21}\times\sqrt{21}$-(Ag,Na) formation, the Si bulk bands (**b**, for example) as well as the surface resonances have shifted by $\sim$0.4 eV to higher binding energy [Fig. 7(b)], indicating that the bulk bands bend downward so that the valence band goes away from E_F. Comparing with the Si(111)$\sqrt{3}\times\sqrt{3}$-Ag surface, the valence band maxima for these two $\sqrt{21}\times\sqrt{21}$ surfaces are estimated to be located at $E_B\sim0.56$ eV, meaning that the E_F is located at the middle of the band gap so that their surface space-charge layers are depletion layers. The bulk band projection regions have shifted downward as depicted by the shaded region in Figs. 7(b)–7(d). Similar changes in band bending to higher binding energy have also been reported for the Cu- or Au- induced $\sqrt{21}\times\sqrt{21}$ phases.[15,40]

At least, six states, S_1–S_6, are found in the bulk band gap for Si(111)$\sqrt{21}\times\sqrt{21}$-Ag, being consistent to the previous reports[11,12] and seven states, $S_1'(S_1'')\sim S_7'$, for Si(111)$\sqrt{21}\times\sqrt{21}$-(Ag,Na) as shown in Fig. 7. One can confirm a close similarity for the overall band structures between the Na- and Ag-induced $\sqrt{21}\times\sqrt{21}$ phases. Around the zone boundary of $\sqrt{21}\times\sqrt{21}$ SBZ [$k\sim1.3$ Å^{-1} in Figs. 7(b) and 7(c)], both surfaces show the band folding for $S_1(S_1')$ and $S_4(S_4')$ and, furthermore, the energy gaps at zone boundaries due to the $\sqrt{21}\times\sqrt{21}$ Bragg reflections (Figs. 2 and 3) have the similar values of 0.1–0.2 eV. It is now obvious that the surface band structures of the Ag- and Na-induced $\sqrt{21}\times\sqrt{21}$ phases are identical to one another and, therefore, their Fermi rings are essentially the same. It is worth noting that the filled STM images of the $\sqrt{21}\times\sqrt{21}$-(Ag,Na) superstructure, shown in Fig. 4 have a close resemblance to those of the $\sqrt{21}\times\sqrt{21}$-Ag and $\sqrt{21}\times\sqrt{21}$-(Ag,Au) superstructures.[12] Concerning the results of Fig. 2, the photoemission signals observed inside the $\sqrt{21}\times\sqrt{21}$ Fermi rings presented in Fig. 2(e) are likely originated from the Na-cluster covered "$\sqrt{3}\times\sqrt{3}$" domain (Fig. 4). Furthermore, clearer spectral appearances of the Fermi rings for Si(111)$\sqrt{21}\times\sqrt{21}$-Ag than those for Si(111)$\sqrt{21}\times\sqrt{21}$-(Ag,Na) are naturally explained by the larger domain size for the former surface than that of the latter one.

Since the adsorbed Ag or a Na atoms provide electrons to the Si(111)$\sqrt{3}\times\sqrt{3}$-Ag surface, their similarity of ionic radius, described in Table I, seems to imply that adsorption sites of monovalent atoms on the surface are mainly governed by the adatom size rather than their electronegativity or the first ionic energy. Furthermore, the similar gap size in the band splitting at the $\sqrt{21}\times\sqrt{21}$ zone boundaries indicates that the amplitude of the $\sqrt{21}\times\sqrt{21}$-periodic potential which is responsible for the Bragg reflection is almost the same between the Ag- and Na-induced $\sqrt{21}\times\sqrt{21}$ phases.[33] According to Table I, ionic radius is a possible criterion to estimate the periodic potentials and ZB gaps. Recently, ARPES measurements on the Si(111)$\sqrt{21}\times\sqrt{21}$-(Ag,Cs) as well as Si(111)$\sqrt{21}\times\sqrt{21}$-(Ag,K) surfaces have been performed.[41,42] The researches have reported that the surface band structures near Fermi level are similar to the present results, but the gaps at zone boundaries are larger ($\sim$0.3 eV). As shown in Table I, K and Cs atoms have larger atomic or ionic radii than Na, which supports our model.

The band structures of the Ag- and Au-induced $\sqrt{21}\times\sqrt{21}$ phases have also shown a close resemblance to each other, and they have been interpreted as modified states of the pristine $\sqrt{3}\times\sqrt{3}$-Ag substrate; the original states are energetically pulled down by electron transfer from the adatoms.[11–13] Since a Na atom is also a monovalent atom as Ag and Au, and since Na has much lower electronegativity than that of Ag or Si, the observed band structure is reasonably ascribed to the same picture.[43] The $S_1(S_1',S_1'')$ and $S_4(S_4',S_4'')$ states of the $\sqrt{21}\times\sqrt{21}$ phases are assigned to the

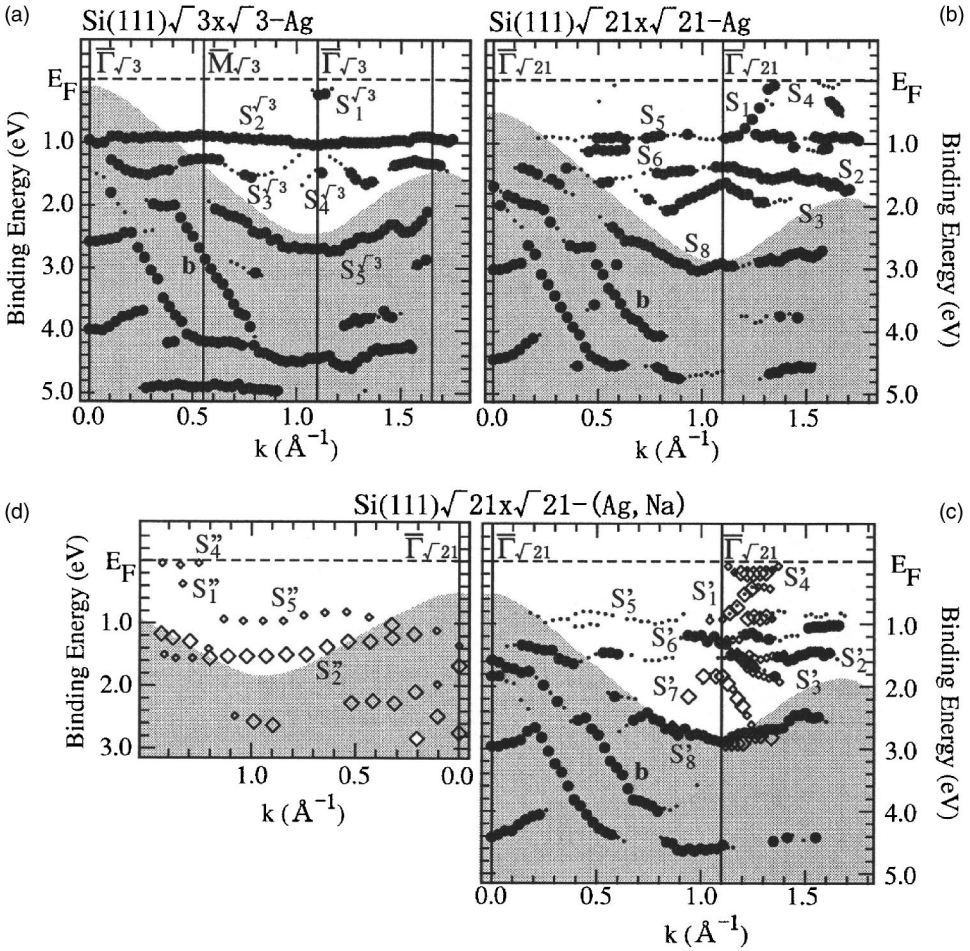

FIG. 7. Experimental dispersions for (a) Si(111)$\sqrt{3}\times\sqrt{3}$-Ag, (b) Si(111)$\sqrt{21}\times\sqrt{21}$-Ag, (c) Si(111)$\sqrt{21}\times\sqrt{21}$-(Ag,Na) along the $[\bar{1}10]$ direction, and for (d) Si(111)$\sqrt{21}\times\sqrt{21}$-(Ag,Na) along the $[11\bar{2}]$ direction. The small and large symbols represent the rather distinctive and the weak spectral features, respectively. Solid circles and open diamonds indicate peak positions obtained by He Iα radiation and synchrotron radiation ($h\nu$=21.2 eV). The shaded region is the bulk band structure projected onto the 1×1 SBZ. (c) and (d) are plotted from ARPES spectra in Fig. 6.

$S_1^{\sqrt{3}}$ state of the original $\sqrt{3}\times\sqrt{3}$-Ag surface that has been pulled down to $E_B\sim0.9$ eV. The $S_2(S_2',S_2'')$ and $S_3(S_3',S_3'')$ surface-state bands have also pulled down compared to the bands of the original $\sqrt{3}\times\sqrt{3}$-Ag surface while the $S_5(S_5',S_6')$ bands appear at the similar E_B's to the pristine $\sqrt{3}\times\sqrt{3}$ bands.[7,11,12,25,26] Although there has been no report on the band assginment for the Si(111)$\sqrt{21}\times\sqrt{21}$-Ag and Si(111)$\sqrt{21}\times\sqrt{21}$-(Ag,Na) surfaces, these facts seem to indicate that the surface states of the $\sqrt{3}\times\sqrt{3}$-Ag surface split into two groups, downward-shifted ones and nonshifted ones, as described in the previous research.[11] According to the recent structure models of the $\sqrt{21}\times\sqrt{21}$ structure, the $\sqrt{3}\times\sqrt{3}$ sites in the $\sqrt{21}\times\sqrt{21}$ unit cell are partially occupied,[14,29,44] implying that there coexists the perturbed and the unperturbed $\sqrt{3}\times\sqrt{3}$ sites. Sites in the superstructure unit cell with and without an adatom may result in the formation of two band groups that have E_B's similar to and different from the original bands. A proper theoretical calculation on the surface structures and surface state bands are highly required to clarify this issue.

Concerning the downward-dispersing S_7' state (which corresponds to the $S_4^{\sqrt{3}}$ in the $\sqrt{3}\times\sqrt{3}$-Ag), the energy position at $\bar{\Gamma}_{\sqrt{21}\times\sqrt{21}}$ point with $k\sim1.1$ Å^{-1} in Fig. 7(c) (which is equivalent to $\bar{\Gamma}_{\sqrt{3}}$ point in Fig. 2) corresponds to the uppermost Si(111) bulk valence band of Λ_3 symmetry at $\bar{\Gamma}$ point with $k=0$, and the dispersion is similar to the bulk band.[37] Thus, the S_7' band dispersion could arise from the surface $\sqrt{3}\times\sqrt{3}$ umklapp scattering of the bulk direct transition. The $S_5^{\sqrt{3}}$ state, which corresponds to the S_8, and S_8' states in the $\sqrt{21}$ phases, may be ascribed to Si back-bond states through comparison among the previous ARPES studies on metal-on-Si surface superstructures.[2] The bands at $E_B\sim4.5$ eV observed within bulk band gap may be Ag 4*d*-related states as previously proposed.[25] As a consequence, the overall band structures are similar among $\sqrt{3}\times\sqrt{3}$-Ag, $\sqrt{21}\times\sqrt{21}$-Ag, and $\sqrt{21}\times\sqrt{21}$-(Ag,Na) superstructures and the difference near E_F is also explained by electron transfer into the $\sqrt{3}\times\sqrt{3}$ bands.

C. Ag 4*d* level

As shown in Fig. 1, two peaks are found at ~5.6 and ~6.4 eV for the $\sqrt{3}\times\sqrt{3}$ phase while two prominent ones at ~5.7 and ~6.8 eV for the two $\sqrt{21}\times\sqrt{21}$ phases. By ARPES measurements of the Ag 4*d* levels, we found that these 4*d* states have little band dispersion. From Fig. 1, one can notice that these two Ag 4*d* peaks for the $\sqrt{21}\times\sqrt{21}$ phase have broader widths and larger energy differences between them than those for the $\sqrt{3}\times\sqrt{3}$ phase. Furthermore, the intensity ratio between the two peaks are also found to vary through the $\sqrt{3}\times\sqrt{3}$-to-$\sqrt{21}\times\sqrt{21}$ phase transformation. Drastic changes of the spectral features clearly indicate notable perturbations of the Ag 4*d* band structures. The origin may

be inferred as (1) significant changes of chemical (physical) environments of Ag atoms in the $\sqrt{3}\times\sqrt{3}$-Ag substrate or (2) additional Ag 4*d* signals from the Ag adsorbates. However, the similar spectral Ag 4*d* features between Si(111)$\sqrt{21}\times\sqrt{21}$-Ag and Si(111)$\sqrt{21}\times\sqrt{21}$-(Ag,Na) as shown in Fig. 1 denies the second possibility.

Concerning electronic bands originated from localized states as *d* orbitals, the modification may be described in terms of variations of Ag-Ag atom distance, which is an important parameter for transfer integrals in the tight-binding approximation.[45] The adsorption seems to induce new chemical bonds between the Ag or Na adatom and Ag atoms composing the $\sqrt{3}\times\sqrt{3}$ framework, resulting in a change of Ag-Ag distance in the Ag trimer. Furthermore, the local variation likely unbalance the $\sqrt{3}\times\sqrt{3}$-Ag atomic configuration, as reported in STM,[48] and, finally, induce significant variations of the Ag—Ag distance or rearrangement of the whole Ag atoms in the $\sqrt{3}\times\sqrt{3}$ substrate. Therefore, the overall spectral feature of Ag 4*d* peaks changes significantly as shown in Fig. 1. The Ag rearrangement was also suggested by x-ray diffraction study.[14] According to the previous researches on the noble-metal induced $\sqrt{21}\times\sqrt{21}$ structures,[13,14] the adatoms are proposed to sit on Ag or Si trimers of the honeycomb chained triangle (HCT) or inequivalent triangle (IET) models.[46,47] The adsorption on the Ag trimer is likely much efficient to induce such Ag arrangement than on the Si trimer. It is also reasonable in terms of the electron transfer described above since a metallic surface state $S_1^{\sqrt{3}}$ of the $\sqrt{3}\times\sqrt{3}$ substrate has large density of states at the Ag trimer.[47] The adsoption site is consistent to a study of the first-principles calculation which has reported that adsorption on the Ag trimer is much stable than on the Si trimer.[44]

D. Surface-state conductivity

One of the intriguing phenomena of the $\sqrt{3}\times\sqrt{3}$-to-$\sqrt{21}\times\sqrt{21}$ transition is its electrical conduction change.[1,16] It has been found that conductivity of the $\sqrt{21}\times\sqrt{21}$ phase is larger than that of the $\sqrt{3}\times\sqrt{3}$ phase.[16,36,49] The previously measured conductivities were originated from three electrical channels of surface-state bands on the topmost atomic layers, bulk-state bands in a surface space-charge layer beneath the surface, and bulk-state bands in the inner crystal. Since the measurements have been performed *in situ* in UHV with the same Si wafer, the transport change is only described in terms of channels except that of a bulk Si. From the band bending change discussed above, an accumulation (inversion) layer formed for the $\sqrt{3}\times\sqrt{3}$ phase on a *p*-(*n*-) type Si wafer becomes a depletion layer when the surface transforms to the $\sqrt{21}\times\sqrt{21}$ phase. Therefore, carriers in the space charge layer are depleted and the conductivity decreases through the $\sqrt{3}\times\sqrt{3}$-to-$\sqrt{21}\times\sqrt{21}$ transition, which is opposite to the experimental fact. Judging from the above, the surface-state channel is responsible for the increase of electrical conductivity and the phenomena is qualitatively explained by increment of carriers in the surface superstructure as found by the present and previous photoemission spectroscopy researches.[1,13,16] We now discuss two-dimensional (2D) electrical conductivity $\sigma_{\sqrt{21}}$ of the $\sqrt{21}\times\sqrt{21}$ phase quantitatively from the measured Fermi surface.

TABLE II. The values of Fermi wave-number k_F, effective mass m^*/m_e, density of state $\mathcal{D}^{2D}$, Fermi velocity v_F, conductivity σ, relaxation time τ, and mean free path l for the Si(111)$\sqrt{3}\times\sqrt{3}$-Ag and the Si(111)$\sqrt{21}\times\sqrt{21}$-Ag surfaces.

	$\sqrt{3}$-Ag	$\sqrt{21}$-Ag
k_F(Å^{-1})	0.10[a]	0.26
m^*/m_e	0.13[a]	0.25
$\mathcal{D}^{2D}$ (10^{13} eV^{-1} cm^{-2})	5.4	10.4
v_F(10^8 cm/s)	0.9	1.2
σ(10^{-4} $\Omega^{-1}/\square$)[b] (meas.)	~0.75	~3.2
τ(10^{-15} s)	~2.2	~2.7
l (Å)	~19	~32

[a]Reference 30.
[b]References 16 and 36.

The relation between the 2D conductivity and Fermi surface is given by the Boltzmann equation as the integral containing the velocity tensor of $v_{ki}v_{kj}$ (See Appendix). Because of the definition $v_{ki}=(1/\hbar)(\partial E/\partial k_i)$, detailed band dispersion curves of the metallic bands at E_F is required to calculate $\sigma_{\sqrt{21}}$. Although the photoemission signals are complicated due to superposition of the Fermi rings of electron and hole pockets as well as those of two domains with rotation of $\pm R10.89°$ as shown in Fig. 2, a summation of all the portions of the Fermi rings of the second and third SBZs produces a single Fermi circle in an extended zone as shown in Fig. 3. As described above, furthermore, the S_4 band dispersion near E_F is fairly reproduced by extrapolation of parabolic fit of the S_1 band dispersion. This approximation is reasonable for the present system since the gap formation at the zone boundaries is so small that it hardly perturbs the energy dispersion at E_F. Since the Si(111)$\sqrt{3}\times\sqrt{3}$-Ag surface has also an isotropic 2D electronic system[30] as shown in Fig. 2, conductivities of both the $\sqrt{3}\times\sqrt{3}$ and $\sqrt{21}\times\sqrt{21}$ superstructures are written by a simple relation as (See the Appendix)

$$\sigma=\frac{e^2}{2}\cdot(\tau\cdot v_F)\cdot v_F\cdot\mathcal{D}^{2D}, \tag{2}$$

where τ is the carrier relaxation time, v_F the Fermi velocity, and $\mathcal{D}^{2D}$ the 2D density of states at E_F. A change in the surface-state conductivity by the transition from the $\sqrt{3}\times\sqrt{3}$-Ag to $\sqrt{21}\times\sqrt{21}$ phases corresponds simply to the difference between $\sigma_{\sqrt{21}}$ and $\sigma_{\sqrt{3}}$ given by Eq. (2) with their individual parameters. Since the two systems are fairly represented by the nearly free-electron model, density of states at Fermi level is written as $\mathcal{D}^{2D}=m^*/\pi\hbar^2$. The Fermi velocity is given as $v_F=\hbar k_F/m^*$. As obtained before, m^* is $0.25m_e$ and k_F is ~0.26 Å^{-1} for Si(111)$\sqrt{21}\times\sqrt{21}$-Ag, where m_e is the free-electron mass. On the other hand, $m^*=0.13m_e$ and $k_F\sim0.1$ Å^{-1} are for Si(111)$\sqrt{3}\times\sqrt{3}$-Ag.[30] From these parameters, one can estimate $\mathcal{D}^{2D}$ and v_F for these two superstructures, which are summarized in Table II. The $\mathcal{D}^{2D}$ and

$v_F(v_F^2)$ of the $\sqrt{21}\times\sqrt{21}$ phase is 92% and 35(83)% larger than those of $\sqrt{3}\times\sqrt{3}$, respectively. As a consequence, the conductivity has become 3.5 times larger through the $\sqrt{3}\times\sqrt{3}$-to-$\sqrt{21}\times\sqrt{21}$ transition.

The previous researches have performed extensive conductivity measurements on the $\sqrt{3}\times\sqrt{3}$-Ag phase and noble-metal induced $\sqrt{21}\times\sqrt{21}$ phases by four-point probe method.[16,36,49] They have found that the surface conductivity has increased by 2×10^{-4} $\Omega^{-1}/\square$ through this structural transformation. With proper calculations on conductivities of space charge layers based on their x-ray photoemission spectroscopy (XPS) results, the experimental surface state conductivity has become 4–6 times larger through the transition.[1,16,36] For an example,[36] conductivities through the $\sqrt{3}\times\sqrt{3}$ and $\sqrt{21}\times\sqrt{21}$ surface superstructures was estimated about 0.75 and 3.2×10^{-4} $\Omega^{-1}/\square$, respectively. The rate of conductivity increase is nearly the same as one obtained from the metallic bands (Fermi surfaces), described above. Therefore, we can naturally explain that conductivity of the $\sqrt{21}\times\sqrt{21}$ superstructure is larger than that of the $\sqrt{3}\times\sqrt{3}$ one because of the higher Fermi velocity and the larger number of Fermi electrons. Inserting the experimental conductivity values in Eq. (2), carrier relaxation time and mean free path of the phases are estimated and listed in Table II. The relaxation time is similar to that reported for the Si(111)4 $\times$1-In surface[19] and one order of magnitude smaller than that in bulk Ag metal at room temperature.[33] As a consequence, the Boltzmann picture reasonably describes the surface state transport of the $\sqrt{3}\times\sqrt{3}$-Ag and $\sqrt{21}\times\sqrt{21}$ phases.

IV. CONCLUSIONS

We have found a $\sqrt{21}\times\sqrt{21}$ surface superstructure by Na deposition of $\sim$0.15 ML coverage at 65–130 K on the Si(111)-$\sqrt{3}\times\sqrt{3}$-Ag surface. We have extensively studied the evolution of electronic structure during the transformation from the $\sqrt{3}\times\sqrt{3}$-Ag to the $\sqrt{21}\times\sqrt{21}$ phases during adsorption of monovalent adsorbates (Ag and Na). Despite the sharp difference of chemical properties between noble and alkali metal adsorbates, the surface electronic structures, Fermi rings, valence bands, and Ag 4*d* levels, show close similarities between the two $\sqrt{21}\times\sqrt{21}$ phases. Through the Fermi surface mapping by ARPES, the $\sqrt{21}\times\sqrt{21}$ phases were found to have the Fermi rings of a hole pocket at the $\bar{\Gamma}$ point and an electron pocket at the $\bar{K}$ point in each reduced surface Brillouin zone. The conductivity of the $\sqrt{21}\times\sqrt{21}$ superstructure is estimated from the measured Fermi surface using the Boltzmann equation and it successfully reproduces the previous transport results.[1,16,36] The adatoms likely sit on Ag trimers of the Si(111)$\sqrt{3}\times\sqrt{3}$-Ag surface and the adsorption is seemingly governed by atomic or ionic radius rather than chemical properties (ionic energy or electronegativity).

ACKNOWLEDGMENTS

M. Ueno, H. Okino, N. Nagamura, K. Motegi, and A. Harasawa are gratefully acknowledged for their help during the experiments. This work has been supported by Grants-In-Aid from the Japanese Society for the Promotion of Science. The experiment on synchrotron radiation is performed at KEK-PF, Japan, with the pac number of 2002G029. M.D. thanks the French Ministry of Foreign Affairs (Bourse Lavoisier) for financial support.

APPENDIX

The relation between the 2D conductivity and Fermi surface is given as follows, based on the Boltzmann equation and assuming a constant relaxation time $\tau=\tau(\mathbf{k})$ irrespective of electron wave-vector $\mathbf{k}$[33,50,51]

$$\sigma_{ij}=\frac{1}{2\pi^2}\frac{e^2\tau}{\hbar}\int\frac{v_{ki}v_{kj}dk_F}{|v_k|}, \tag{A1}$$

where k_F and $v_{ki}=(1/\hbar)(\partial E/\partial k_i)$ are the Fermi wave vector and Fermi velocity along *i* direction, respectively. The integral is done on the Fermi surface.

If a surface state can be regarded as an isotropic free-electronlike state, $|v_{ki}|=|v_{kj}|=|v_k|=v_F$ at E_F and the Boltzmann equation is written as

$$\sigma=\frac{e^2\pi v_F^2}{4\pi^2\hbar}\int\frac{dk_F}{|v_k|}, \tag{A2}$$

$$=\frac{e^2\pi v_F}{4\pi^2\hbar}\int dk_F. \tag{A3}$$

Two-dimensional density of states $\mathcal{D}^{2D}$ per area at Fermi level is given as

$$\mathcal{D}^{2D}=\frac{1}{2\pi^2}\int\frac{dk_F}{|\partial E/\partial k|}, \tag{A4}$$

$$=\frac{1}{2\pi^2\hbar}\int\frac{dk_F}{|v_k|}. \tag{A5}$$

and σ is simply rewritten as

$$\sigma=\frac{e^2}{2}\cdot(\tau\cdot v_F)\cdot v_F\cdot\mathcal{D}^{2D}. \tag{A6}$$

It is an important consequence of the Boltzmann equation that σ is proportional to relaxation time (τ), Fermi velocity (v_F), density of states at Fermi level ($\mathcal{D}^{2D}$), and mean free path $l(=\tau\cdot v_F)$. In the Boltzmann regime, surface electron transport is governed by the number and velocity of 2D Fermi electrons.

If we adopt (nearly) free-electron approximation, the integral in Eq. (A3) and electron density in the surface-state band n_{2D} are given as

$$\int dk_F=2\pi k_F, \tag{A7}$$

$$n_{2D}=\frac{1}{2\pi^2}(\pi k_F^2). \tag{A8}$$

From these parameters with $k_F=m^*v_F/\hbar$ in Eq. (A3), σ defined by the Boltzmann equation is expressed by the Drude formula

$$\sigma = \frac{e^2 \pi n_{2D}}{m^*}, \tag{A9}$$

$$= e\mu n_{2D}. \tag{A10}$$

In the Drude regime, surface electron transport is expressed by (total) electron density in the surface-state band n_{2D} and mobility $\mu(=e\tau/m^*)$.[33,50,51] Despite the simplicity of the Drude formula compared to the Boltzmann equation, the latter formula has much generality to describe electron transport and we adopt the formula (A6) for the discussion.

*Electronic address: matsuda@surface.phys.s.u-tokyo.ac.jp

[1] S. Hasegawa, X. Tong, S. Takeda, N. Sato, and T. Nagao, Prog. Surf. Sci. **60**, 89 (1999).

[2] R. I. G. Uhrberg and G. V. Hansson, Crit. Rev. Solid State Mater. Sci. **17**, 133 (1991).

[3] K. D. Lee and J. Chung, Phys. Rev. B **57**, R2053 (1998).

[4] I. Matsuda, H. W. Yeom, K. Tono, and T. Ohta, Phys. Rev. B **59**, 15784 (1999).

[5] J. Nogami, Surf. Rev. Lett. **1**, 395 (1994).

[6] S. Hasegawa, N. Sato, I. Shiraki, C. L. Petersen, P. Boggild, T. M. Hansen, T. Nagao, and F. Grey, Jpn. J. Appl. Phys., Part 1 **39**, 3815 (2000).

[7] I. Matsuda, H. Morikawa, C. Liu, S. Ohuchi, S. Hasegawa, T. Okuda, T. Kinoshita, C. Ottaviani, A. Cricenti, M. Dangelo, P. Soukiassian, and G. LeLay, Phys. Rev. B **68**, 085407 (2003).

[8] T. Takahashi, H. Tajiri, and K. Sumitani, Surf. Rev. Lett. **10**, 519 (2003).

[9] Y. Nakajima, S. Takeda, T. Nagao, S. Hasegawa, and X. Tong, Phys. Rev. B **56**, 6782 (1997).

[10] J. N. Crain, K. N. Altmann, C. Bromberger, and F. J. Himpsel, Phys. Rev. B **66**, 205302 (2002).

[11] H. M. Zhang, K. Sakamoto, and R. I. G. Uhrberg, Phys. Rev. B **64**, 245421 (2001).

[12] X. Tong, S. Ohuchi, N. Sato, T. Tanikawa, T. Nagao, I. Matsuda, Y. Aoyagi, and S. Hasegawa, Phys. Rev. B **64**, 205316 (2001).

[13] X. Tong, C. S. Jiang, and S. Hasegawa, Phys. Rev. B **57**, 9015 (1998).

[14] H. Tajiri, K. Sumitani, W. Yashiro, S. Nakatani, T. Takahashi, K. Akimoto, H. Sugiyama, X. Zhang, and H. Kawata, Surf. Sci. **493**, 214 (2001).

[15] X. Tong, C. S. Jiang, K. Horikoshi, and S. Hasegawa, Surf. Sci. **449**, 125 (2000).

[16] S. Hasegawa, J. Phys.: Condens. Matter **12**, R463 (2000).

[17] C. Liu, I. Matsuda, H. Morikawa, H. Okino, T. Okuda, T. Kinoshita, and S. Hasegawa, Jpn. J. Appl. Phys., Part 1 **42**, 4659 (2003).

[18] T. Tanikawa, I. Matsuda, R. Hobara, and S. Hasegawa, e-J. Surf. Sci. Nanotechnol. **1**, 50 (2003).

[19] T. Kanagawa, R. Hobara, I. Matsuda, T. Tanikawa, Akiko Natori, and S. Hasegawa, Phys. Rev. Lett. **91**, 036805 (2003).

[20] I. Matsuda, M. Ueno, T. Hirahara, R. Hobara, H. Morikawa, C. Liu, and S. Hasegawa, Phys. Rev. Lett. **93**, 236801 (2004).

[21] J. J. Paggel, G. Neuhold, H. Haak, and K. Horn, Surf. Sci. **414**, 221 (1998).

[22] D. R. Lide, *CRC Handbook of Chemistry and Physics, 2002-2003: A Ready-Reference Book of Chemical and Physical Data (CRC Handbook of Chemistry and Physics, 83rd Ed)* (CRC, Boca Raton, 2002).

[23] M. Ueno, I. Matsuda, C. Liu, and S. Hasegawa, Jpn. J. Appl. Phys., Part 1 **42**, 4894 (2003).

[24] R. I. G. Uhrberg, H. M. Zhang, T. Balasubramanian, E. Landemark, and H. W. Yeom, Phys. Rev. B **65**, 081305 (2002).

[25] T. Yokotsuka, S. Kono, S. Suzuki, and T. Sagawa, Surf. Sci. **127**, 35 (1983).

[26] L. S. O. Johansson, E. Landemark, C. J. Karlsson, and R. I. G. Uhrberg, Phys. Rev. Lett. **63**, 2092 (1989).

[27] T. Okuda, K. Sakamoto, H. Nishimoto, H. Daimon, S. Suga, T. Kinoshita, A. Kakizaki, Phys. Rev. B **55**, 6762 (1997).

[28] T. Okuda, H. Shigeoka, H. Daimon, S. Suga, T. Kinoshita, and A. Kakizaki, Surf. Sci. **321**, 105 (1994).

[29] M. D'angelo, I. Matsuda, M. Konishi, C. Liu, H. Morikawa, and S. Hasegawa, Surf. Sci. (to be published).

[30] T. Hirahara, I. Matsuda, M. Ueno, and S. Hasegawa, Surf. Sci. **563**, 191 (2004).

[31] T. Hirahara, I. Matsuda, and S. Hasegawa, e-J. Surf. Sci. Nanotechnol. **2**, 141 (2003).

[32] J. Voit, L. Perfetti, F. Zwick, H. Berger, G. Margaritondo, G. Grüner, H. Höchst, and M. Grioni, Science **290**, 501 (2000).

[33] N. W. Ashcroft and N. D. Mermin, *Solid State Physics* (Saunders College Publishing, Harcourt Brace College Publishers, Florida, 1976).

[34] S. Kono, K. Higashiyama, T. Kinoshita, T. Miyahara, H. Kato, H. Ohsawa, Y. Enta, F. Maeda, and Y. Yaegashi, Phys. Rev. Lett. **58**, 1555 (1987).

[35] X. Tong, C. S. Jiang, K. Horikoshi, and S. Hasegawa, Surf. Sci. **449**, 125 (2000).

[36] C.-S. Jiang, X. Tong, S. Hasegawa, and S. Ino, Surf. Sci. **376**, 69 (1997).

[37] R. I. G. Uhrberg, G. V. Hansson, J. M. Nicholls, P. E. S. Persson, and S. A. Flodström, Phys. Rev. B **31**, 3805 (1985).

[38] H. J. Neff, I. Matsuda, M. Hengsberger, F. Baumberger, T. Greber, and J. Osterwalder, Phys. Rev. B **64**, 235415 (2001).

[39] I. Matsuda, M. Hengsberger, F. Baumberger, T. Greber, H. W. Yeom, and J. Osterwalder, Phys. Rev. B **68**, 195319 (2003).

[40] S. Hasegawa, C. S. Jiang, Y. Nakajima, and T. Nagao, Surf. Rev. Lett. **5**, 803 (1998).

[41] C. Liu *et al.*, (unpublished).

[42] H. M. Zhang, K. Sakamoto, and R. I. G. Uhrberg, Phys. Rev. B **70**, 245301 (2004).

[43] M. Konishi, I. Matsuda, C. Liu, H. Morikawa, T. Okuda, T. Konishita, and S. Hasegawa, e-J. Surf. Sci. Nanotechnol. **3**, 107 (2005).

[44] H. Aizawa and M. Tsukada, Phys. Rev. B **59**, 10923 (1999).

[45] W. A. Harrison, *Electronic Structure and the Properties of Solids*

(Dover, New York, 1989).
[46] T. Takahashi, S. Nakatani, Surf. Sci. **282**, 17 (1993).
[47] H. Aizawa, M. Tsukada, N. Sato, and S. Hasegawa, Surf. Sci. **429**, L509 (1999).
[48] N. Sato, T. Nagao, and S. Hasegawa, Phys. Rev. B **60**, 16083 (1999).
[49] X. Tong, S. Hasegawa, and S. Ino, Phys. Rev. B **55**, 1310 (1997).
[50] W. Jones and N. H. March, *Theoretical Solid State Physics Volume 2* (Dover, New York, 1985).
[51] T. Heinzel, *Mesoscopic Electronics in Solid State Nanostructures* (Wiley-VCH, New York, 2003).